ACS APPLIED BIO MATERIALS

www.acsabm.org Article

Polymer Brush-Grafted Nanoparticles Preferentially Interact with Opsonins and Albumin

Nikolaus Simon Leitner, Martina Schroffenegger, and Erik Reimhult*

Cite This: *ACS Appl. Bio Mater.* 2021, 4, 795−806 Read Online

ACCESS | Metrics & More | Article Recommendations | Supporting Information

ABSTRACT: Nanoparticles find increasing applications in life science and biomedicine. The fate of nanoparticles in a biological system is determined by their protein corona, as remodeling of their surface properties through protein adsorption triggers specific recognition such as cell uptake and immune system clearance and nonspecific processes such as aggregation and precipitation. The corona is a result of nanoparticle−protein and protein−protein interactions and is influenced by particle design. The state-of-the-art design of biomedical nanoparticles is the core−shell structure exemplified by superparamagnetic iron oxide nanoparticles (SPIONs) grafted with dense, well-hydrated polymer shells used for biomedical magnetic imaging and therapy. Densely grafted polymer chains form a polymer brush, yielding a highly repulsive barrier to the formation of a protein corona *via* nonspecific particle−protein interactions. However, recent studies showed that the abundant blood serum protein albumin interacts with dense polymer brush-grafted SPIONs. Herein, we use isothermal titration calorimetry to characterize the nonspecific interactions between human serum albumin, human serum immunoglobulin G, human transferrin, and hen egg lysozyme with monodisperse poly(2-alkyl-2-oxazoline)-grafted SPIONs with different grafting densities and core sizes. These particles show similar protein interactions despite their different "stealth" capabilities in cell culture. The SPIONs resist attractive interactions with lysozymes and transferrins, but they both show a significant exothermic enthalpic and low exothermic entropic interaction with low stoichiometry for albumin and immunoglobulin G. Our results highlight that protein size, flexibility, and charge are important to predict protein corona formation on polymer brush-stabilized nanoparticles.

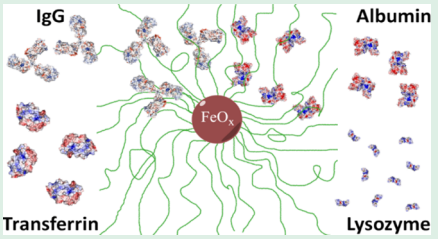

KEYWORDS: *core−shell nanoparticle, protein corona, protein adsorption, isothermal titration calorimetry, poly(2-ethyl-2-oxazoline), poly(2-alkyl-2-oxazoline)*

INTRODUCTION

Core−shell nanoparticles are an exciting tool for many current and future biomedical applications.[1−4] They are biphasic composite materials consisting of an inner core and an outer shell with different material properties. An inorganic core, for example, iron oxide, can be used as a contrast agent for bioimaging or as a signal-transducing element for *in vivo* biosensing, while a polymeric, porous, or vesicle core can act as a storage and release vessel for drug delivery.[3,5] The physicochemical properties of a nanoparticle determine their usefulness in these respects and decide their biological fate.[6,7] These properties are highly dependent on the shape, size, and type of the material and, therefore, extremely sensitive to aggregation with other particles or macromolecules in the environment.[6,8]

It is well established that biomolecules in biofluids adsorb immediately onto the surface of the nanoparticles.[9,10] The dominant molecules adsorbing to and altering the properties of the nanoparticles are proteins, which is why this layer was named the protein corona by Cedervall *et al.*[11] Our understanding of the importance of the protein corona has evolved dramatically over the last decade.[12] Today, it is understood as the single most crucial factor to determine the fate and, therefore, the efficacy of nanoparticles in medical applications.[11,13] Proteins with high affinity to a nanoparticle form a dense and irreversibly adsorbed "hard protein corona". In contrast, proteins with low affinity form a loosely bound "soft protein corona" in equilibrium with the bulk.[6,11,14−16] The "hard corona" is easy to analyze, while only little is known about the amount and identity of proteins in the "soft corona" because of the low affinity and weak binding of the involved proteins.[17]

Major contributions have been made to our understanding of how physicochemical parameters of the surface of a nanoparticle influences which proteins are incorporated into the corona and how thick the corona is.[12,18] This has led to the consensus that nanoparticles for biomedical applications require a hydrophilic surface coating that entropically penalizes protein adsorption, with polymer brushes as the leading

Received: October 19, 2020
Accepted: December 13, 2020
Published: December 29, 2020

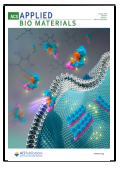

candidates to fulfill this role.[12] The highly hydrated polymer brush forms a steric barrier. It gives rise to a repulsive hydration force that screens attractive van der Waals (vdW) and charge interactions between the core and biomolecules if the shell is sufficiently thick and dense.[19,20] An example of this concept used in the biomedical field is superparamagnetic iron oxide nanoparticles (SPIONs) with a hydrophilic polymer shell. They are considered low-toxic and biocompatible nanomaterials suitable as magnetic resonance contrast agents[21,22] for hyperthermia cancer therapy[23,24] or separation of biomolecules.[25] We[26−28] and others[29,30] have demonstrated that SPIONs stabilized with irreversibly grafted and dense polymer brush shells can exhibit outstanding colloidal stability in biological media. Further, the suppression of the SPION−protein and SPION−cell membrane interaction correlated with negligible uptake of nanoparticles by various phagocytic cells *in vitro*.[26−28]

Intravenous injection is still considered the most important and effective administration form for medical nanoparticles.[5,31] Thus, the adsorption of serum proteins on nanoparticles is of the highest interest and relevance.[20] Nonspecifically adsorbed proteins in the corona can lead to reduced bioavailability and also trigger specific uptake and transport. Certain adsorbed and intact transport proteins, such as transferrin, have been reported to lead to increased intracellular uptake by cells,[31,32] while adsorption of opsonins is believed to increase clearance by the immune system. The "Vroman effect" describes how the protein species in the protein corona is changing over time. Blood serum is a protein-rich environment, and abundant proteins, such as albumin, IgG, and fibrinogen, will adsorb first and will later be replaced by proteins with a lower dissociation constant (K_D).[32,33] In a protein-poor environment, such as the lungs, abundant proteins such as albumin and transferrin dominate the protein corona also in the late phase.[34] Nanoparticles rapidly circulate the vasculature. Thus, the early stages of the protein corona formed in the protein-rich blood environment are likely decisive for the fate of intravenously injected nanoparticles, which adds urgency to understanding which blood proteins associate with stealth nanoparticles because of abundancy or high affinity.[20]

Isothermal titration calorimetry (ITC) measures the heat given up or needed by chemical-, enzymatic-, or binding interactions as a function of relative concentration.[35−37] The heat of binding of a substrate to its binding partner is integrated per injection to obtain the binding enthalpy (ΔH). The dissociation constant (K_D) (or the Gibbs free energy, ΔG) and the stoichiometry of binding (n) are extracted by fitting a model for the binding interaction to the titration curve. These parameters are relatively insensitive to the experimental conditions, while the accuracy of the determination of the binding enthalpy (ΔH) and entropy (ΔS) is sensitive to the affinity, concentration, and stoichiometry of the reactants during the measurements.[38−40] ITC is heavily used in enzyme research, as well as to determine receptor and transport protein interactions in drug discovery. It has also been applied to investigating the binding of protein coronas to nanoparticles with differently tailored surface interactions,[15,41,42] but there are fewer examples of its application to the more demanding task of quantifying the interaction of nanoparticles designed to suppress the binding of proteins.[18,43]

We recently used ITC to show that bovine serum albumin adsorbs to SPIONs, even when they are grafted with dense linear polymer brushes that provide them with perfect colloidal stability and negligible cell uptake.[43] ITC possessed sufficient sensitivity to quantify the nonspecific association to the core−shell SPION of, on average, ∼1 albumin per particle with an adsorption energy of <10 k_BT. Such partial soft coronas could still be decisive for outcomes *in vivo* and deserve further investigation. In follow-up work, we demonstrated that human serum albumin (HSA) adsorption is completely suppressed on SPION with a brush shell architecture using cyclic topology compared to the traditional linear brush-stabilized particles ubiquitously in use.[44,45] This architecture densifies the shell close to the nanoparticle's core and suggests that protein−core interactions are not entirely screened even for densely grafted linear brush particles. It is still unclear whether the adsorption takes place to the core, in the shell, or onto the dense brush, but the attractive interactions between proteins and particles occur with the core. While the association with albumin has been implicated in prolonging circulation times of drug delivery vehicles *in vivo* and could be beneficial, association with other proteins, such as opsonins, could significantly affect uptake and biodistribution of nanoparticles and be decidedly detrimental to biomedical applications.[43] Until now, a quantitative study on the weak adsorption of different kinds of proteins on stealth polymer brush-grafted nanoparticles is missing.

In this work, we quantify the nonspecific interaction between four serum proteins (albumin, immunoglobulin G, transferrin, and lysozyme) and SPIONs grafted with thermoresponsive, methyl-terminated poly(2-alkyl-2-oxazoline) (PAOZ) shells. This SPION design should be resistant to protein adsorption in the hydrated state of PAOZ, that is, below the critical solution temperature (CST) of the grafted polymer.[28] Recent findings of immunogenic effects due to heavy dosing of nanoparticles stabilized with poly(ethylene glycol) (PEG) leading to decreased blood circulation times[10,32,46,47] have led to a search for alternatives to PEG.[10,47] We choose poly(2-ethyl-2-oxazoline) (PEtOZ) and poly(2-ethyl-2-oxazoline)-*co*-poly(2-isopropyl-2-oxazoline) (PEtIOZ) as a substitute because of their similar properties to PEG below the CST in suppressing protein interactions and their ability to change solubility as a function of temperature. The thermoresponsiveness of PAOZ allows the design of true "smart" nanoparticles capable of triggered cell attachment and detachment or targeted drug delivery.[43,48,49] Two different SPIONs were synthesized to highlight the impact of different polymer brush densities and particle sizes. The same average number of polymer chains was grafted onto spherical monodisperse iron oxide cores of different diameters, leading to disparate grafting densities. Both SPIONs show high colloidal stability, but only the particles with the higher grafting density are known to show suppressed uptake by phagocytic cells.[26−28,50−52]

We selected four proteins for their relevance to biomedical applications. Albumin, immunoglobulin G (IgG), and transferrin are globulins found in abundance in serum. Lysozyme is a secreted enzyme with a very low concentration in blood serum.[53] It was chosen as a low-molecular-weight protein to probe whether a small size is instrumental to protein adsorption into dense polymer shells. Albumin on nanoparticles can promote phagocytosis, despite its use to prolong the circulation of therapeutic molecules.[9,32] IgG is an opsonin that triggers phagocytosis and activation of the complement system.[9,54] Even if the IgG does not recognize and bind specifically to the nanoparticles, their nonspecific adsorption

https://dx.doi.org/10.1021/acsabm.0c01355
ACS Appl. Bio Mater. 2021, 4, 795−806

will trigger the same activation. Transferrin controls iron transport to the cytoplasm, and it has been suggested to influence transport across the cell membrane when adsorbed to the nanoparticle surface.[31,32]

MATERIALS AND METHODS

Materials. All chemicals used in the nanoparticle synthesis were purchased from Merck and used as received unless otherwise indicated. The exceptions were (1-cyano-2-ethoxy-2-oxoethylidenaminooxy)dimethylamino-morpholino-carbenium hexafluorophosphate (COMU) that was purchased from Carl Roth, 2-ethyl-2-oxazoline that was dried over CaH_2 before use, and methyl-*p*-toluenesulfonate that was distilled before use. (4-(2-Hydroxyethyl)-1-piperazineethanesulfonic acid) (HEPES), NaCl, KCl, recombinant human serum albumin, hen egg lysozyme, human transferrin, and human immunoglobulin G (IgG) from serum were purchased from Sigma-Aldrich. Regenerated cellulose 0.22 μm syringe filters were purchased from Bruckner Analysentechnik.

Synthesis of SPIONs. The synthesis of oleic acid-coated SPION followed established protocols.[32,33] Briefly, iron oxide nanoparticles were synthesized by thermal decomposition of iron(0)pentacarbonyl in dioctyl ether in the presence of oleic acid, leading to highly monodisperse, spherical, single-crystal iron oxide nanoparticles. The molar ratio between iron(0)pentacarbonyl and oleic acid determines the size of the resulting particles. By increasing the amount of oleic acid, the size of the nanoparticles will also increase.[32,55]

Polymerization of 2-Ethyl-2-oxazoline to Poly(2-ethyl-2-oxazoline) (PEtOZ). 2-Ethyl-2-oxazoline (4 mL, 39 mmol) was dissolved in 12 mL of dimethylacetamide (DMA) under an inert atmosphere. Methyl *p*-tosylate (29 μL, 0.19 mmol) was added to the reaction solution. The reaction was stirred for 16 h at 100 °C. Afterward, the reaction was quenched with 400 μL of water at 70 °C for another 5 h. The quenching with water introduces a terminal OH-group. The final product was precipitated with a 1:1 (v/v) mixture of diethyl ether and hexane and dried under vacuum. A quantitative yield of 4.7 g was obtained. The molecular weights were determined with gel permeation chromatography (GPC) and were 22,900 g/mol with a polydispersity index (PDI) of 1.12.

Polymerization of 2-Ethyl-2-oxazoline and 2-Isopropyl-2-oxazoline to Poly(2-ethyl-2-oxazoline-*co*-2-isopropyl-2-oxazoline) (PEtIOZ). 2-Isopropyl-2-oxazolnie (2.5 mL, 21 mmol) and 2-ethyl-2-oxazoline (0.2 mL, 2 mmol) were dissolved in 8 mL of DMA under an inert atmosphere. Methyl *p*-tosylate (30 μL, 0.2 mmol) was added to the reaction solution. The reaction was stirred for 16 h at 100 °C. Afterward, the reaction was quenched with 200 μL of water at 70 °C for another 5 h. The quenching with water introduces a terminal OH-group. The final product was precipitated with a 1:1 (v/v) mixture of diethyl ether and hexane and dried under vacuum. A quantitative yield of 4.7 g was obtained. The molecular weights were determined with GPC and were 18,285 g/mol with a PDI of 1.06.

Functionalization of PAOZ. As an example, 4.7 g (0.14 mmol) of hydroxy-terminated poly(2-ethyl-2-oxazoline) was dissolved in 20 mL of dry chloroform. Succinic anhydride (219 mg, 2.2 mmol) and 4-(dimethylamino) pyridine (89 mg, 0.7 mmol) were added to the reaction mixture. The reaction was refluxed for 24 h. The carboxylic acid-terminated product was precipitated with a mixture of diethyl ether and hexane (1/1: v/v). Yield: 4.2 g (89%). PEtOZ was end-functionalized with nitrodopamine (NDA) because of its high affinity to Fe(III), forming bonds of a near-covalent characteristic.[25,36] Amide coupling of 6-nitrodopamine to the carboxylic acid-terminated polymer was carried out by dissolving 4.2 mg (0.18 mmol) of carboxylic acid-terminated poly(2-ethyl-2-oxazoline) in 50 mL of dry DMF under an inert atmosphere. Subsequently, COMU (235 mg, 0.55 mmol) and diisopropylethylamine (0.3 mL, 1.7 mmol) were added. Carboxylic acid was activated for 10 min, after which we added the NDA (201 mg, 0.68 mmol). The reaction mixture was stirred for 24 h. The product was precipitated from diethyl ether and hexane (1/1: v/v) and dialyzed for 3 days with a cutoff 3.5 kDa. The poly(2-ethyl-2-oxazoline)-*co*-poly(2-isopropyl-2-oxazoline) was functionalized analogously. Yield NDA-PEtOZ: 3.2 g, 76%; functionalization 100%, NDA-PEtIOZ: 1.7 g, 87, functionalization 65.5%. NMR: ^{1}H NMR for poly(2-ethyl-2-oxazoline)-NDA δH (300 MHz; MeDO) 7.53 (1H, s, Ar−H), 6.73 (1H, s, Ar−H), 4.27 (2H, CH_2OCO-), 3.70−3.20 (4nH, $-N-CH_2CH_2-$ polymer), 2.60−2.25 (2nH, CH_2CH_3, polymer), 1.30−0.95 (3nH, CH_2CH_3, polymer) (Figures S1).

^{1}H NMR for poly(2-ethyl-2-*co*-2-isopropyl-2-oxazoline)-NDA δH (300 MHz; $CDCl_3$) 7.61 (1H, s, Ar−H), 6.71 (1H, s, Ar−H), 4.27 (2H, CH_2OCO-), 3.70−3.20 (4nH, $-N-CH_2CH_2-$ polymer), 3.0−2.50 (1nH, CH_2CH_3, polymer), 2.50−2.20 (2nH, CH_2CH_3, polymer) 1.30−0.95 (6nH, $(CH_2CH_3)_2$, polymer and (3nH, CH_2CH_3, polymer), ratio between EtOZ and IOZ:13:87 (Figure S2).

Characterization of PAOZ. The ^{1}H NMR spectra of polymers were obtained on a BRUKER AV III 300 MHz spectrometer. Chemical shifts were recorded in ppm and referenced to a residual protonated solvent [$CDCl_3$: 7.27 ppm (1H) and MeOD: 3.31 (1H)]. Polymer molecular weights were determined by GPC on a Malvern Viscotek GPCmax system with three MZ Gel SDPlus columns (a precolumn, followed by two columns with separation ranges of 10−2000 and 1−40 kDa, respectively) (Figure S3). A Knauer Smartline RI Detector 2300 detected the difference in the refractive index. Dimethylformamide (DMF) with 0.05 LiBr was used as eluent. Samples (50 μL) with a concentration of 3 g/L were injected and measured at 60 °C at a flow rate of 0.5 mL/min. Polystyrene standards of 1.5−651 kg/mol were used for external calibration. The analysis was performed with the OminSEC 5.12 software.

Grafting of NDA-Functionalized PAOZ to Iron Oxide Cores. Wet iron oxide nanoparticles (with an inorganic fraction of 10 weight-%) were dissolved in 0.5 mL of toluene. PAOZ (1 g) terminated with NDA was dissolved in 12 mL of DMF. Both solutions were mixed and sonicated for 24 h. The product was precipitated with diethyl ether and hexane (1/1: v/v) and dialyzed for 3 days with a cutoff of 100 kDa to remove all excess dispersant. The 5 nm cores were grafted with NDA-PEtOZ. The 8 nm cores were grafted with NDA-PEtIOZ.

Characterization of PAOZ-Grafted SPIONs. Transmission electron micrographs were recorded on an FEI Tecnai G2 with a 160 kV acceleration voltage on carbon-coated grids. Nanoparticle size distributions were calculated with the freeware Pebbles[40] based on the analysis of >1000 NPs (Figures S4 and S5). Thermogravimetric analysis (TGA) of the core−shell nanoparticles was performed on a Mettler Toledo TGA/DSC with 80 mL/min synthetic air as the reactive gas, 20 mL/min nitrogen as a protective gas, and a heating rate of 10 K/min from 25 to 650 °C (Figures S6 and S7). Mass loss from 150 to 500 °C was assigned to the polymer shell, while the residual mass was attributed to the inorganic core. The mass loss was corrected for the losses recorded up to 150 °C, which are due to moisture or solvent residues. The grafting density, σ, was calculated using

$$\sigma = \frac{\frac{(\%\ w/w)_{shell}}{(\%\ w/w)_{core}} \rho_{ironoxide} V_{core} N_A}{M_{ligand} A_{core}}$$

where σ is the grafting density, $(\%\ w/w)_{shell}$ is the percentage of mass loss in TGA for the organic fraction corresponding to the ligand shell, N_A is the Avogadro constant, $\rho_{iron\ oxide}$ is the density of iron oxide, V_{core} is the volume, A_{core} is the area of the iron oxide core calculated from the diameter of the cores measured by TEM, M_{ligand} is the molecular weight of the ligand, and $(\%\ w/w)_{core}$ is the residual mass percentage of the inorganic fraction in TGA.

Dynamic Light Scattering Measurements. The hydrodynamic diameters (D_H) of the particles were measured with a Malvern Zetasizer Nano-ZS dynamic light scattering (DLS) device (Malvern Panalytical Ltd, Malvern, UK). The mass concentration of particles in HEPES-BS buffer was 10 μg/mL, and the measurements were performed at 25 °C. Each reported distribution is an average of 30 runs, and the CONTIN algorithm was used to extract the number-weighted size distributions.

https://dx.doi.org/10.1021/acsabm.0c01355
ACS Appl. Bio Mater. 2021, 4, 795−806

Preparation of Iron Oxide Core−Shell Nanoparticle Dispersions and Protein Solutions. From 2.4 g of HEPES, 8 g of NaCl, and 0.2 g KCl in a final volume of 1 L of Milli-Q water, HEPES-buffered saline (HEPES-BS) was prepared, yielding a final concentration of 137 mM NaCl, 10 mM HEPES, and 2.7 mM KCl. The pH was adjusted to 7.4 by the addition of NaOH. The buffer was filtered with a 0.22 μm syringe filter, sterilized at 121 °C and 2 bar, and stored at 4 °C. Before use, the buffer was degassed for 20 min using a sonicator (Elma Transsonic T 460 bath sonicator), equilibrated to 25 °C for 10 min using a water bath, and filtered again through a 0.22 μm syringe filter. An analytic balance (Sartorius Secura Micro Balance) was used to weigh particles and proteins. HEPES-BS was used to dissolve the proteins and disperse the particles to the stock concentrations used in the measurements described below. All particle dispersions were produced fresh and used the same day.

Isothermal Titration Calorimetry. A Malvern Panalytical MicroCal Auto-iTC200 system was used for the titration experiments. The ITC cell was filled with a 1 μM particle dispersion. The protein solutions acted as titrants and were used in a concentration range between 62.5 and 250 μM. Sixteen titrations were performed per sample at 25 °C. Before the first injection, the baseline was recorded for 20 min. The first injection had a volume of 0.5 μL and was removed from the data evaluation. The volumes of the remaining injections were 2 μL. The spacing between two injections was 500 s until the eighth injection and 280 s after the ninth injection. The stirring speed was 1000 rpm, and the reference power was 41.8 μW. The "one set of identical binding sites"-model was used for data analysis. This model assumes that all possible binding sites on the particle are independent and have the same K_D and ΔH. It is equivalent to using the Langmuir model to analyze nonspecific adsorption. We deemed it to be the best assumption for modeling the nonspecific binding to polymer brush-stabilized nanoparticles. For baseline correction, the "Fitted Offset" mode was applied, where a constant control heat is assumed and fitted to the integrated heat along with the fitting parameters of the "one set of identical binding sites" model.

Computing Protein Properties. The ProtParam[56] tool of the Swiss Institute of Bioinformatics was used for the computation of physicochemical protein properties, such as theoretical pI, instability index, aliphatic index, and the grand average of hydropathicity. Swiss-Prot/TrEMBL accession numbers P02768, P01863, P02787, and P61626 were used as models for HSA, IgG, transferrin, and lysozyme.

RESULTS AND DISCUSSION

Iron oxide core nanoparticles of two different diameters were synthesized and grafted with PAOZ polymer brushes. A schematic of the synthesis strategy is provided in Figure S8. Example TEM micrographs used for the calculation of the core size distributions are shown in Figure 1. The core size distributions determined from a large set of transmission electron micrographs are shown in Figures S4 and S5. The monodisperse spherical cores visible in the transmission electron micrographs facilitate a precise calculation of the grafting density and the number of NDA-PAOZ chains per nanoparticle from the total organic fraction determined by TGA (Figures S6 and S7).

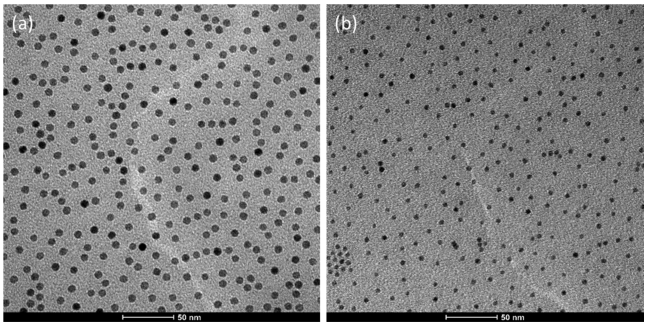

Figure 1. Transmission electron micrographs of the cores used for (a) 8nm FeO-PEtIOZ and (b) 5nm FeO-PEtOZ core−shell nanoparticles.

By grafting a similar number of NDA-PAOZ (~90 chains) and almost the same polymer mass per core, we obtained nanoparticles that have significantly different grafting densities because of their different surface areas (Table 1). Therefore, at the same particle molarity, also the polymer molarities in the samples are virtually identical. The particles with the larger iron oxide core (8nm FeO-PEtIOZ) have 0.46 chains per nm^{-2}, while the particles with the smaller core (5nm FeO-PEtOZ) have 1.10 chains per nm^{-2}. By this choice, we can investigate how the protein adsorption to the particles depends on the density of the polymer shell. The interaction of a protein with the nanoparticle results from the balance of the attractive interactions of the core and the repulsive potential of the polymer brush. A polymer brush provides a repulsive potential to colloidal (protein) adsorption over the distance of the brush if the polymer does not interact attractively with the protein on the molecular level. The absence of affinity between the proteins and the free PAOZ polymers is shown in Figures S9 and S10 (also see Figure S11 for the control injection of protein to pure HEPES-BS), where the same polymer molarity (85 μM) is applied as in the nanoparticle interaction measurements by ITC. Therefore, the hydrated polymer brush contributes a repulsive osmotic potential and sterically blocks access to the core surface, as previously demonstrated.[20,43,44] However, the core displays a range of possible attractive vdW, charge, and hydrophobic interactions. Without a polymer brush, iron oxide nanoparticles rapidly aggregate and sediment in aqueous or protein dispersion (data not shown).[21,57,58] Hence, we will only avoid aggregation if the iron oxide core's attractive interactions to another particle or a protein are weaker or shorter range than the repulsive PAOZ−brush interaction. This can, for example, be observed by the colloidal stability of the PAOZ-grafted nanoparticles in DLS measurements (Figure S12).

Hen egg lysozyme, recombinant human serum albumin, human transferrin, and human IgG were chosen to have relevant serum proteins with different sizes, masses, and functions (Table 2). Under biological conditions, HSA and transferrin have a negative, lysozyme a positive, and IgG a balanced net charge. There are no significant differences in the aliphatic index between these four proteins.

The repulsive potential of polymer brushes is, on average, high, but especially for strongly curved nanoparticles, inhomogeneities in the grafting density could lead to locally accessible defects. Such defects could also dynamically appear and disappear as the local polymer density fluctuates with the highly mobile polymer chains. We expected that smaller proteins such as lysozyme and albumin should more easily adsorb inside the polymer brush at such points of locally lower polymer density and repulsion when compared to larger proteins such as IgG. At low polymer brush density, even the polymer brush's average repulsive potential will be too low to screen out the core's attractive potential. Summarizing both effects, we hypothesized that a denser polymer brush should experience lower nonspecific protein interaction than less dense brushes.[59] Further, we hypothesized that small and

https://dx.doi.org/10.1021/acsabm.0c01355
ACS Appl. Bio Mater. 2021, 4, 795−806

Table 1. Characteristics of Iron Oxide Nanoparticles Grafted with PAOZ

sample	core diameter [nm]	molar mass of the grafted polymer [kg mol^{-1}]	grafting density, σ [chains nm^{-2}]	molar mass particle [kg mol^{-1}]	D_H [nm]	full width at half-maximum [nm]
5nm FeO-PAOZ	5.0	23	1.1	2220	26 ± 1	11 ± 1
8nm FeO-PAOZ	7.8	18	0.46	2594	25 ± 3	11 ± 2

Table 2. Properties of the Blood Serum Proteins Used to Study the Interactions with Iron Oxide Nanoparticles Grafted with PAOZ

name	type	average mass [kDa]	average concentration in human blood [μM]	titrant concentration [μM]	$pI_{theoretical}$[a]	II[a]	AI[a]	GRAVY[a]
lysozyme	secreted	14.4	1.5×10^{-4}	250	9.3	32	70	−0.49
albumin	albumin	67	600	125−250	5.7	39	77	−0.40
transferrin	β-globulin	75−81	30	125	6.7	38	70	−0.41
IgG	γ-globulin	150	7	62.5−250	7.2	44	74	−0.34

[a]Values derived from the ProtParam tool. pI—isoelectrical point; II—instability index; AI—aliphatic index; and GRAVY—grand average of hydropathicity.

dynamic proteins should demonstrate higher nonspecific adsorption than large and inflexible proteins.[59]

The attractive DLVO interactions between proteins and polymers or nanoparticles are highly dependent on the amino acid composition, protein conformation, and post-translational modifications such as glycosylation. Because of this sensitivity and the sensitivity to other competing adsorbing species, it is important to measure well-characterized and pure samples. Initial ITC experiments on recombinant human lysozyme produced irreproducible measurements (see Figure S13). Most likely, the sometimes weak and sometimes absent interactions stemmed from glycoside impurities. Therefore, we replaced human lysozyme with hen egg lysozyme, which could be obtained in pure form.

ITC has been proven to be an excellent method for the study of nanoparticle−biomolecule interactions.[43] It allows for the direct and fast testing of "stealth" properties of core−shell particles. Figures 2 and 3 show the injection plots of ITC measurements of the interaction of (a) transferrin, (b) hen egg lysozyme, (c) HSA, and (e) human IgG with 5 nm core (Figure 2) and 8 nm core (Figure 3) PAOZ-grafted nanoparticles. The smaller core particles, 5 nm FeO-PAOZ, shown in Figure 2, display different interactions depending on the injected protein. Figure 2a−c,e shows the differential power (DP) as a function of injection and time for each of the proteins.

We directly observe that the interaction between the different proteins and 5 nm FeO-PAOZ particles can be grouped into two classes. The transferrin and lysosome injections show small and predominantly positive peaks (Figure 2a,b) almost indistinguishable from those observed for all proteins injected to the free polymer (*cf.* Figures S9 and S10). A positive injection peak means an endothermic reaction. In these cases, the mainly endothermic response followed by a minor exothermic peak is not attributed to an endothermic interaction between the proteins and the particles. The response is due to the heat of dilution, which is an artifact caused by the dilution of the protein solution in the dispersion in the calorimetric bomb. This is demonstrated by comparing to the injection of the proteins to pure buffer (Figure S11). We, therefore, conclude that these two proteins do not adsorb a corona or, in any other significant way, interact with the polymer-grafted nanoparticles.

In contrast, the HSA and IgG show large negative injection peaks that swamp the heat of dilution (Figure 2c,e). It demonstrates a significant binding of these two proteins to the nanoparticles. This qualitative observation can be made quantitative by replotting the data as the enthalpy change per injection by the integration of the DP for each injection peak as a function of the molar ratio (Figure 2d,f). The enthalpy *versus* molar ratio plots are used for the determination of the number of binding sites (n), the dissociation constant (K_D), and the thermodynamic parameters (ΔG, ΔH, and ΔS) by fitting a sigmoidal function to the data. The fitted function corresponds to the assumption of equal (nonspecific) binding sites for the proteins on the nanoparticles, and it appears to reproduce these data sets well. The binding stoichiometry (n) and the dissociation constant K_D are derived directly from the plot fit. ΔG is calculated as $\Delta G = RT \ln K_D$ and ΔS as $\Delta S = (\Delta H - \Delta G)/T$, where R is the gas constant and T is the temperature.[60]

Although ΔG and n can be determined with reasonable accuracy also at the molar ratios and binding energies observed here, ΔH and ΔS cannot be determined with high accuracy according to the criterion given by that a Wiseman c-value of $c = n[M]/K_D > 2$ should be achieved, where $[M]$ is the concentration of the nanoparticles.[40] In our measurements, we have $c \sim 0.29-2.25$, which is at the limit of what can be achieved for these nanoparticles. Only the nanoparticle concentration can be tweaked, but the volume fraction and viscosity become too high if the concentration is increased to allow for rapid mixing and to avoid higher-order colloidal interactions. However, Tellinghuisen demonstrated that a reliable fit for K_D (ΔG) could be achieved even for values of $c < 10^{-4}$[40] and that the analysis is insensitive to errors in the determination of n at very low c.[39] The results from the fits are given in Table 3 for HSA and Table 4 for IgG. The relatively large errors expected for ΔH and ΔS can be observed for the samples with low c-values. As transferrin and lysozyme did not show binding interactions with any of the nanoparticles, their data were not fitted.

The affinity of HSA to the 5 nm FeO-PAOZ nanoparticles is significant with a dissociation constant of $K_D = 3.1$ μM, but with very few proteins binding per particle ($n = 2.2$). Although the measurements are quantitatively more uncertain, the larger 8 nm FeO-PAOZ nanoparticles have an order of magnitude higher dissociation constant of $K_D = 34$ μM and several times higher number of proteins binding per particle ($n = 7.0$).

Nonspecific binding can be strong because of the multivalent nature of the interactions. That the number of proteins

https://dx.doi.org/10.1021/acsabm.0c01355
ACS Appl. Bio Mater. 2021, 4, 795−806

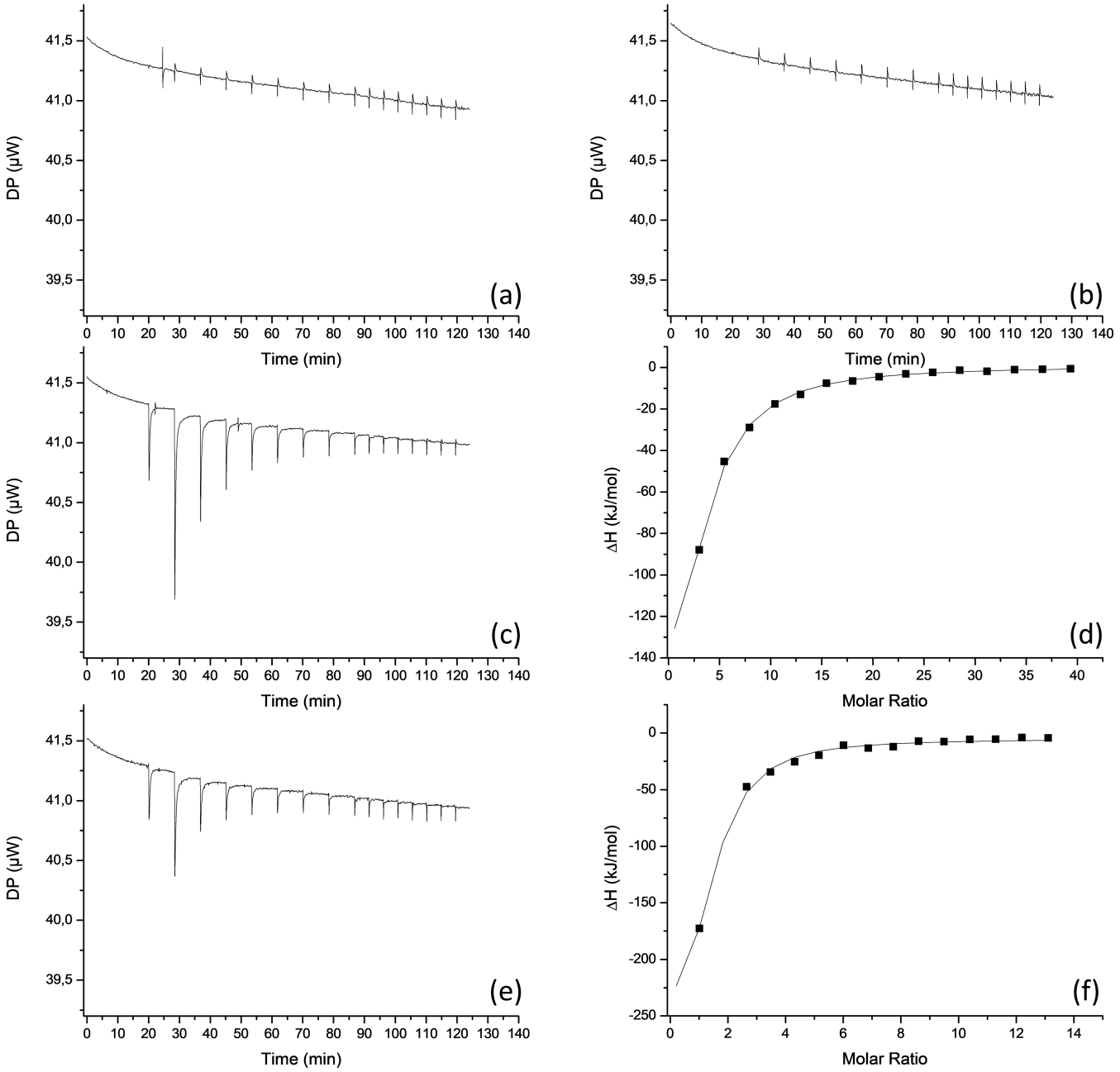

Figure 2. ITC measurements of the titration of serum proteins to core−shell nanoparticles with high polymer brush grafting density. (a) DP of the injection of transferrin to 1 μM of 5 nm core diameter iron oxide nanoparticles grafted with 23 kg mol^{-1} linear PAOZ (5 nm FeO-PAOZ) with 1.1 chains/nm^{-2} and (b) DP of the injection of lysozyme to 5 nm FeO-PAOZ (1 μM). (c) DP of the injection of HSA to 5 nm FeO-PAOZ (1 μM) and (d) enthalpy per injection and fitting of the Weisman model (solid line). (e) DP of the injection of IgG to 5 nm FeO-PAOZ (1 μM) and (f) enthalpy per injection and fitting of the Weisman model (solid line).

bound per 5 nm FeO-PAOZ particle is on the order of 1 means that the nature of the protein association is different from the concept of the protein corona. The relatively weakly bound and very few proteins per such particle are in agreement with that their dense polymer brushes have been shown sufficient for stealth-like properties.[26−28,61] Approximately 10 proteins bound on the nanoparticle surface, as for the 8 nm FeO-PAOZ, could be considered a corona-like coating for a nanoparticle of this small size. The result for 8 nm FeO-PAOZ could explain why nanoparticles with polymer grafting densities of similar polymers below σ < 0.7 have shown decisively worse stealth performance *in vitro* than particles with grafting densities on the level of the 5 nm FeO-PAOZ. In neither case does the protein adsorption trigger additional protein−protein aggregation, given the low aggregation number and the colloidal stability of the samples in the presence of serum proteins.

It seems likely that the associated proteins are bound to defects in the polymer brush coating where the core can be accessed rather than associated generally with the polymer brush shell. This mode of interaction is also expected from that the proteins do not interact with the polymer even at high concentrations (*cf.* Figures S9 and S10). The higher binding stoichiometry of HSA to the nanoparticles with the larger cores

https://dx.doi.org/10.1021/acsabm.0c01355
ACS Appl. Bio Mater. 2021, 4, 795−806

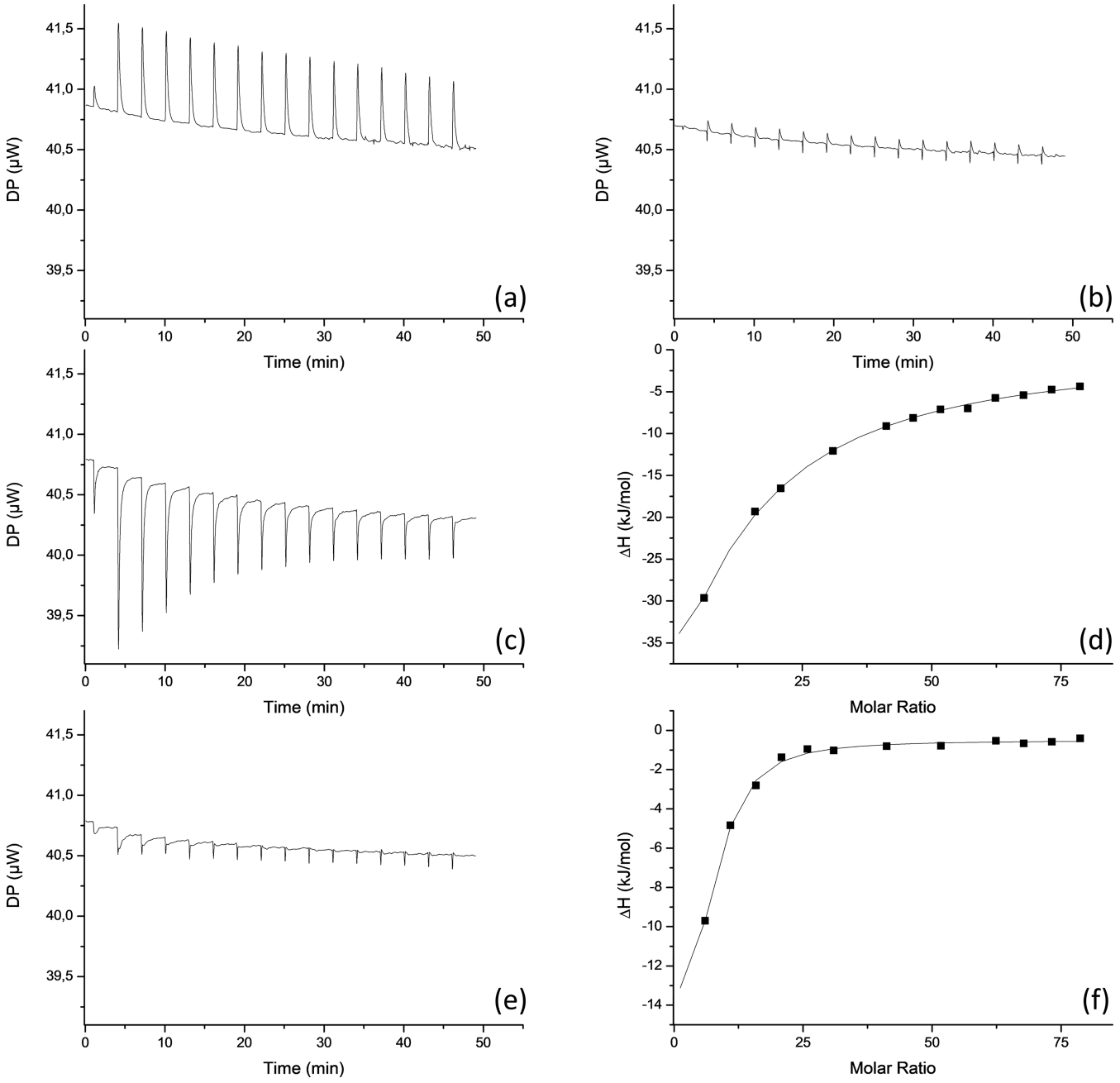

Figure 3. ITC measurements of titration of serum proteins to core−shell nanoparticles with intermediate polymer brush grafting density. (a) DP of the injection of transferrin to 1 μM of 8 nm core diameter iron oxide nanoparticles grafted with 18 kg mol^{-1} linear PAOZ (8 nm FeO-PAOZ) with 0.46 chains/nm^{-2} and (b) DP of the injection of lysozyme to 8 nm FeO-PAOZ (1 μM). (c) DP of the injection of HSA to 8 nm FeO-PAOZ (1 μM) and (d) enthalpy per injection and fitting of the Weisman model (solid line). (e) DP of the injection of IgG to 8 nm FeO-PAOZ (1 μM) and (f) enthalpy per injection and fitting of the Weisman model (solid line).

Table 3. Thermodynamic Parameters for the Interaction between Recombinant HSA and PAOZ-Grafted Iron Oxide Nanoparticles Calculated by Fitting the ITC Data Using the "One Set of Sites" (Langmuir) Binding Model

sample	binding sites, n	K_D [μM]	ΔG [kJ mol^{-1}]	ΔH [kJ mol^{-1}]	ΔS [kJ mol^{-1} K^{-1}]
5 nm FeO-PAOZ	2.2 ± 0.8	3.1 ± 0.6	−31.6 ± 0.1	−320 ± 140	−1.0 ± 0.5
8 nm FeO-PAOZ	7.0 ± 10	34 ± 18	−25.6 ± 0.6	−240 ± 540	−0.7 ± 0.9

is consistent with the picture that a larger surface area would provide more binding sites. The attractive core surface area increases by a factor of 2.5 per particle, even if the overall nanoparticle size only changes marginally (*cf.* Table 1). This effect, leading to an expectation of more binding sites per particle, should be considered in addition to the lower polymer grafting density on the 8 nm FeO-PAOZ nanoparticles that seems to explain the observations.

The higher K_D, that is, lower binding strength, is more surprising than the stoichiometry of binding. However, it could

https://dx.doi.org/10.1021/acsabm.0c01355
ACS Appl. Bio Mater. 2021, 4, 795−806

Table 4. Thermodynamic Parameters for the Interaction between Human IgG and PAOZ-Grafted Iron Oxide Nanoparticles Calculated by Fitting the ITC Data Using the "One Set of Sites" (Langmuir) Binding Model

sample	binding sites, n	K_D [μM]	ΔG [kJ mol^{-1}]	ΔH [kJ mol^{-1}]	ΔS [kJ mol^{-1} K^{-1}]
5 nm FeO-PAOZ	1.1 ± 0.7	1.6 ± 0.5	−34.1 ± 0.03	−340 ± 250	−1.0 ± 0.6
8 nm FeO-PAOZ	0.9 ± 0.2	0.4 ± 0.2	−36.5 ± 0.01	−110 ± 30	−0.26 ± 0.01

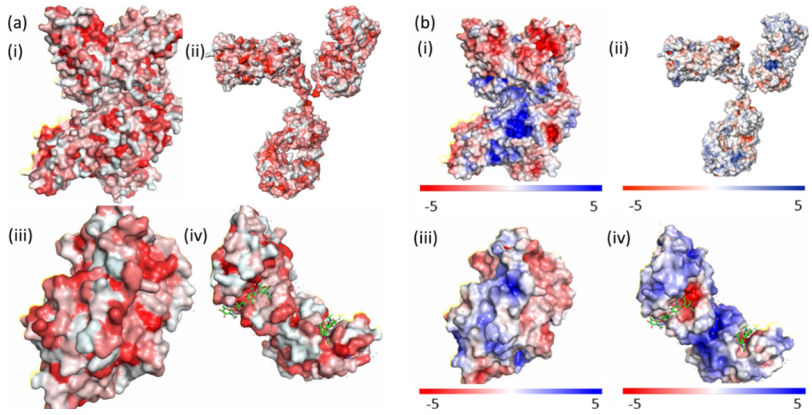

Figure 4. Molecular model representations of the proteins used for the interaction studies. PyMOL 2.0 software and the "Color h" script and APBS were used to visualize the hydrophobicity and electrostatic potentials of the protein surfaces. (a) Hydrophobicity heatmaps. A darker red shade indicates a higher hydrophobicity index. (i) Albumin, (ii) immunoglobulin G, (iii), transferrin, and (iv) lysozyme. Small molecules, such as ions and oligosaccharide residues, are shown in green. (b) Electrostatic potential normalized to k_BT/e, with k_B the Boltzmann constant, T the temperature, and e the elementary charge. Red sections on the surface favor interactions with a positively charged surface and blue sections with a negatively charged surface. (i) Albumin, (ii) immunoglobulin G, (iii), transferrin, and (iv) lysozyme. Small molecules, such as ions and oligosaccharide residues, are shown in green.

be that the lower grafting density allows more defects and points of contact of proteins to the core surface but that most of these binding sites are small and dispersed in the polymer brush. A small average footprint per bound protein means an on-average weaker nonspecific binding strength. The corollary would be that there are different types of defect sites present on the polymer-functionalized nanoparticles, which agree with the observation of higher variability in the measurements. One kind of defect site allows a high degree of access to the particle surface for strong binding, and in a dilute shell, there are also smaller defects at which weaker binding can occur. The presence of two types of binding sites with different origins could contribute to the larger errors in the determination of the thermodynamic parameters observed for 8 nm FeO-PAOZ exposed to HSA. The lower grafting density may lead to higher variability in the density and size of defect sites per nanoparticle that the HSA can bind to. That HSA is a protein with many sub-domains joined by soft linkages known to support its binding to many different substrates[62] undoubtedly facilitates its ability to bind strongly to the nanoparticle core through small defects in the polymer brush shell. Compared to the precision of the other data, it is likely that we are observing a more diverse range of particle interactions than a large measurement error in this experiment, which results in higher uncertainty in the result as we, for simplicity, fit our data to a single−site interaction model.

Although the dissociation constants and stoichiometries are similar, it is notable that both are lower for IgG than for HSA. IgG is a much larger protein and an opsonin with well-known "sticky" domains. We, therefore, expected that IgG would bind both stronger and in higher numbers to the nanoparticles even if the antibody only interacts with the nanoparticle through nonspecific interactions. Reducing the association of IgG to nanoparticles is much more important than suppressing HSA binding, as IgG is an opsonin and signals foreign objects for removal to the immune system. In contrast, albumins were used to prolong the circulation of various biologics.

The lower stoichiometry of IgG than HSA could be related to their relative sizes, which could allow HSA to penetrate and deform more easily into the shell to form more and closer nonspecific interactions with the core surface than IgG can. On the other hand, we observe that IgG binds with higher affinity than HSA and that the affinity constant changes little as a function of particle core size. The stoichiometry of the binding and the dissociation constant remain at $n \sim 1$ and $K_D \sim 1$ μM, respectively. The lack of size dependence for the interaction of the nanoparticles with IgG could also be rationalized by the hypothesis of two types of defect binding sites. Our results are consistent with that all particles possess large defect sites corresponding to those where both HSA and IgG bind at an approximately 1:1 stoichiometry, for which large protein size and stickiness yield a high binding affinity. Additionally, an inadequately dense brush makes it possible for smaller sticky proteins such as HSA to bind to additional sites with lower affinity. In contrast, large and less deformable proteins such as IgG are still shielded from binding to the surface by the dilute polymer brush.

Thus, from the comparison of HSA and IgG, protein size seems to matter in terms of exploiting chinks in the polymer brush armor of the nanoparticles. On the other hand, we did not observe any binding of lysozyme, which is the smallest tested protein, for either of the particles. This result strongly suggests that steric access to the surface is not the sole determining factor. The physicochemical properties of proteins in relation to the properties of the nanoparticle core still matter to exploit incompleteness in the steric-osmotic shield provided by the PAOZ polymer brush; the type of interaction with the core surface matters. The interplay between nonprotected

https://dx.doi.org/10.1021/acsabm.0c01355
ACS Appl. Bio Mater. 2021, 4, 795−806

nanoparticles and protein properties for protein adsorption has been documented.[12,63,64]

The quantitative determination of ΔH and ΔS is uncertain because of the low c for the titration, but some observations regarding the general type of interaction can still be made from the data. The enthalpic and entropic changes appear quite balanced. While changes in the enthalpy are considered an indication of changes in hydrogen and/or vdW bonding, entropy changes stem mainly from hydrophobic interactions and/or conformational changes. Hydrophobic interactions can be ruled out between a well-hydrated polymer and a protein. Still, they could take place with residual hydrophobic ligands left from the synthesis in the innermost part of the shell. There are previous reports regarding the challenge to replace oleate by other ligands from iron oxide nanoparticles under conditions similar to those used in our protocol,[65,66] which make it possible that some oleate is still present in the inner part of the shell. Remaining oleate would both comprise defects where the PAOZ is not grafted and adsorption sites that would be entropically favored. However, the core surface that could have hydrophobic characteristic is limited to a small fraction, given the high average grafting density of PAOZ. Therefore, only small entropy changes are observed for the binding of both proteins. The highly exothermic enthalpy changes in the interaction of HSA with both particles are most likely a manifestation of vdW bonding. As ΔS is negative, a more ordered system must result from the particle−protein interaction. Higher order is an indication that the conformational changes resulting from protein binding and distortions to the shell lead to a more hydrophobic surface and confined protein and polymer conformational space.

Three-dimensional heatmaps of the hydrophobicity (Figure 4a) and the electrostatic potentials (Figure 4b) of the protein surfaces were computed with PyMol applying the "Color h" script[67] and the "Adaptive Poisson-Boltzmann Solver"[68] to elucidate further why the proteins interacted so differently with the nanoparticles. The hydrophobicity maps (Figure 4a) of the proteins used in this study show a large fraction of relatively hydrophobic residues clustered on the surface. Generally, all proteins have hydrophobic patches on their surface that can aid binding to surfaces that are not strongly hydrophilic by displacing water and initiating conformational changes that expose further hydrophobic residues from the interior of the protein. Lysozyme appears slightly less hydrophobic on the surface [Figure 4a(iv)], and it has a significantly smaller hydrophobic interior than the other proteins because of its low molecular weight. The binding of the larger proteins seems enthalpically dominated (Tables 3 and 4), but entropic contributions from displaced water could still be important for the balance of the net interaction. A recent report demonstrated that large proteins could bind entropically instead of enthalpically to bare silica nanoparticles because of their size,[63] which is not observed in our case. In contrast, the interactions are enthalpic and weak. The lower overall hydrophobicity of lysozyme could be part of the explanation why, despite its small size and likely ability to penetrate the polymer shell, it does not bind to the nanoparticles. As the smallest protein, lysozyme also has the lowest vdW attraction to the nanoparticle, which favors the expulsion of lysozyme from the surface driven by the repulsive potential of the PAOZ brush.

Entropic interactions for the polymer-grafted core−shell nanoparticles are long-range unfavorable (osmotic brush repulsion) and only favorable upon direct contact with the core (displacement of water). However, vdW long-range attraction is always driving protein adsorption. We cannot expect major differences in the vdW attraction to the nanoparticles between the similarly sized HSA and transferrin. Conformational flexibility and shape could explain the differences in the ability to penetrate through the shell to bind, which would favor HSA and support the results, given the flexibility of the HSA subdomains internally.[62] The long-range double-layer interaction could further explain why HSA binds strongly to the nanoparticles while transferrin does not. The nonspecific double-layer interaction depends on the electrostatic potential of the surfaces of colloids. IgG and transferrin both seem to have less-charged surfaces than HSA (Figure 4b). Both are only slightly above their pKa (*cf.* Table 2), meaning that their surface potentials should be net negative, but only weakly so. Some transferrins were even reported to have net cationic charge at physiological pH.[69] In contrast, HSA has a high negative surface potential at physiological pH (*cf.* Table 2).[62] The anionic charge is relevant to the interaction with our nanoparticles as our previous work revealed a double-layer interaction at very low ionic strength corresponding to a net positive surface potential of the core of this type of core−shell nanoparticle.[26] The double-layer interaction resulting from the core surface potential is weak and completely screened by the polymer brush shell at physiological pH.[26] As HSA penetrates defects in the shell, it can experience the nonscreened double-layer attraction that is not detectable on the surface of the shell. Transferrin is comparable to HSA in size but less flexible and at least not strongly negatively charged, which together explain why both the PAOZ-stabilized nanoparticles resist transferrin but not HSA adsorption. In contrast, lysozyme has a pKA above physiological pH (*cf.* Table 2) and high cationic surface potential.[70] Lysozyme will, therefore, experience strong double-layer repulsion within the shell. Our results show that this additional repulsive contribution is sufficient to prevent protein adsorption *via* vdW and hydrophobic interactions even for nanoparticles grafted with medium-dense polymer brushes against small proteins such as a lysozyme.

We performed the experiments by exposing the nanoparticles to one protein at a time to establish the thermodynamic equilibrium for protein binding at sequentially higher concentrations. However, by comparing the dissociation constant of each protein and our analysis of the likely properties resulting in protein binding, one can also conclude something about the protein corona formation over time for nanoparticles in blood serum. With HSA binding relatively strongly and being in high abundance, we would expect the protein corona of this type of nanoparticles first to form with ∼1 HSA binding per particle. As time goes by, other proteins that are flexible and negatively charged can additionally add to the corona, although the high concentration of albumin ensures that the few proteins associated with a densely polymer-grafted core−shell nanoparticle will continue to be dominated by HSA. As the proteins compete for the same binding sites, and we have determined the thermodynamic parameters for binding, longer exposure will not lead to an increase in the corona.

CONCLUSIONS

By quantitatively measuring the interaction of a pool of four blood serum proteins with nanoparticles that have different

https://dx.doi.org/10.1021/acsabm.0c01355
ACS Appl. Bio Mater. 2021, 4, 795−806

levels of stealth polymer coatings, we could determine several factors that influence protein adsorption onto polymer-grafted iron oxide nanoparticles. The generic nature of these factors makes them essential to consider for all similarly structured nanoparticles for biomedical or biotechnological applications. This is especially true considering the state-of-the-art polymer brush shells used to make our biomedical iron oxide nanoparticles colloidally stable in biological media and their demonstrated high performance in *in vitro* assays.

It is clear from our results that even nanoparticles with >1 20-kDa-PAOZ-chain nm^{-2} have defects in the polymer brush shell that allow proteins that are small or have flexible domains to penetrate close to the core surface. Once inside the shell, the screening and steric hindrance are not sufficient to suppress attractive DLVO interactions with the core. We observe that when there is a residual attractive double-layer interaction, this is sufficient to drive strong adsorption to such defects but that a repulsive double-layer interaction is sufficient to avoid adsorption in combination with the shell repulsion. From the comparison between HSA, IgG, and transferrin, it seems that just avoiding an attractive double-layer interaction can be sufficient if the protein does not have flexible subdomains.

HSA is not only the most abundant protein in blood serum; we also found that it has strong nonspecific enthalpic interactions with polymer brush-grafted nanoparticles. However, as albumin has been used to improve stealth properties of surfaces, the average binding of ∼1 HSA per particle with a dense polymer brush might not compromise the circulation and biodistribution of such particles *in vivo*. More troubling could be the complete albumin corona that can form on less densely polymer-grafted (still brush-stabilized) nanoparticles and that opsonins such as IgG also demonstrated significant but weaker binding to PAOZ-grafted nanoparticles. IgG is large and does not experience a net strong double-layer attraction from the core even at close range. However, its flexible subdomains provide it with the opportunity to penetrate smaller defects than the total molecular weight suggests.

IgG and similar opsonins are much less abundant than HSA and could, according to our results, be outcompeted by HSA in the blood; this would support the low cell uptake and long circulation times observed for similar polymer-stabilized nanoparticles. Therefore, although our results show that core−shell nanoparticles stabilized by linear polymer brushes currently are not a perfect design, they could produce the desired outcomes of low nonspecific cell uptake and immune system recognition *in vivo*. They also suggest that further improvements should make sure that a shell density is achieved that precludes any dynamic defects from being present in the shell or that no residual charge is present on the core surface or in the brush. These lessons also apply to other common core−shell designs stabilized by polymer brushes that are used for biomedical particles, such as micellar and liposomal drug delivery systems.

■ ASSOCIATED CONTENT

Supporting Information

The Supporting Information is available free of charge at https://pubs.acs.org/doi/10.1021/acsabm.0c01355.

^{1}H NMR spectra, GPC profiles, pebble size analysis of iron oxide NPs, TGA thermographs of FeO-PAOZ particles, synthesis schematic, ITC titration curves of free polymer with buffer and serum proteins, ITC titration of buffer with serum proteins, DLS measurement of particles, and ITC titration of buffer and FeO-PAOZ particles with human lysozyme (PDF)

■ AUTHOR INFORMATION

Corresponding Author

Erik Reimhult − *Institute for Biologically Inspired Materials, Department of Nanobiotechnology, University of Natural Resources and Life Sciences, Vienna A-1190, Austria;* orcid.org/0000-0003-1417-5576; Email: erik.reimhult@boku.ac.at

Authors

Nikolaus Simon Leitner − *Institute for Biologically Inspired Materials, Department of Nanobiotechnology, University of Natural Resources and Life Sciences, Vienna A-1190, Austria;* orcid.org/0000-0003-0507-6357

Martina Schroffenegger − *Institute for Biologically Inspired Materials, Department of Nanobiotechnology, University of Natural Resources and Life Sciences, Vienna A-1190, Austria;* orcid.org/0000-0002-0797-7370

Complete contact information is available at: https://pubs.acs.org/10.1021/acsabm.0c01355

Author Contributions

E.R. and N.S.L. designed the study. M.S. synthesized the nanoparticles. N.S.L. performed all the experiments. N.S.L. and E.R. analyzed the data and wrote the manuscript. All authors reviewed the manuscript.

Funding

The research presented in that paper was funded by the Austrian Science Fund (FWF) grant no. I3064.

Notes

The authors declare no competing financial interest.

■ ACKNOWLEDGMENTS

This project was supported by EQ-BOKU VIBT GmbH through access to the TGA and the ITC at the BOKU Core Facility for Biomolecular and Cellular Analysis. The authors thank Irene Schaffner and Jakob Wallner for the support with ITC and Max Willinger for support with additional sample measurements for the revision.

■ ABBREVIATIONS

SPION, superparamagnetic iron oxide nanoparticles; vdW, van der Waals;; PEtOZ, poly(2-ethyl-2-oxazoline); PEtIOZ, poly-(2-ethyl-2-oxazoline)-*co*-poly(2-isopropyl-2-oxazline); PAOZ, poly(2-alkyl-2-oxazoline); PEG, poly(ethylene glycol); IgG, immunoglobulin G; HSA, human serum albumin; HEPES, (4-(2-hydroxyethyl)-1-piperazineethanesulfonic acid); BS, buffered saline; NDA, nitrodopamine; DLS, dynamic light scattering; ITC, isothermal titration calorimetry

■ REFERENCES

(1) Bobo, D.; Robinson, K. J.; Islam, J.; Thurecht, K. J.; Corrie, S. R. Nanoparticle-Based Medicines: A Review of FDA-Approved Materials and Clinical Trials to Date. *Pharm. Res.* **2016**, *33*, 2373−2387.

(2) Kim, E. H.; Ahn, Y.; Lee, H. S. Biomedical Applications of Superparamagnetic Iron Oxide Nanoparticles Encapsulated within Chitosan. *J. Alloys Compd.* **2007**, *434*−*435*, 633−636.

(3) Anselmo, A. C.; Mitragotri, S. Nanoparticles in the Clinic. *Bioeng. Transl. Med.* **2016**, *1*, 10−29.
(4) Chatterjee, K.; Sarkar, S.; Jagajjanani Rao, K.; Paria, S. Core/Shell Nanoparticles in Biomedical Applications. *Adv. Colloid Interface Sci.* **2014**, *209*, 8−39.
(5) Zhang, L.; Gu, F.; Chan, J.; Wang, A.; Langer, R.; Farokhzad, O. Nanoparticles in Medicine: Therapeutic Applications and Developments. *Clin. Pharmacol. Ther.* **2008**, *83*, 761−769.
(6) Feliu, N.; Docter, D.; Heine, M.; del Pino, P.; Ashraf, S.; Kolosnjaj-Tabi, J.; Macchiarini, P.; Nielsen, P.; Alloyeau, D.; Gazeau, F.; Stauber, R. H.; Parak, W. J. In vivo degeneration and the fate of inorganic nanoparticles. *Chem. Soc. Rev.* **2016**, *45*, 2440−2457.
(7) McClements, D. J.; Xiao, H. Potential Biological Fate of Ingested Nanoemulsions: Influence of Particle Characteristics. *Food Funct.* **2012**, *3*, 202−220.
(8) Ghosh Chaudhuri, R.; Paria, S. Core/Shell Nanoparticles: Classes, Properties, Synthesis Mechanisms, Characterization, and Applications. *Chem. Rev.* **2012**, *112*, 2373−2433.
(9) Knop, K.; Hoogenboom, R.; Fischer, D.; Schubert, U. S. Poly(Ethylene Glycol) in Drug Delivery: Pros and Cons as Well as Potential Alternatives. *Angew. Chem., Int. Ed.* **2010**, *49*, 6288−6308.
(10) Qi, Y.; Chilkoti, A. Protein-polymer conjugation - moving beyond PEGylation. *Curr. Opin. Chem. Biol.* **2015**, *28*, 181−193.
(11) Cedervall, T.; Lynch, I.; Lindman, S.; BerggÅrd, T.; Thulin, E.; Nilsson, H.; Dawson, K. A.; Linse, S. Understanding the nanoparticle-protein corona using methods to quantify exchange rates and affinities of proteins for nanoparticles. *PNAS* **2007**, *104*, 2050−2055.
(12) Ke, P. C.; Lin, S.; Parak, W. J.; Davis, T. P.; Caruso, F. A Decade of the Protein Corona. *ACS Nano* **2017**, *11*, 11773−11776.
(13) Lima, T.; Bernfur, K.; Vilanova, M.; Cedervall, T. Understanding the Lipid and Protein Corona Formation on Different Sized Polymeric Nanoparticles. *Sci. Rep.* **2020**, *10*, 1129.
(14) Gref, R.; Lück, M.; Quellec, P.; Marchand, M.; Dellacherie, E.; Harnisch, S.; Blunk, T.; Müller, R. H. "Stealth" corona-core nanoparticles surface modified by polyethylene glycol (PEG): influences of the corona (PEG chain length and surface density) and of the core composition on phagocytic uptake and plasma protein adsorption. *Colloids Surf., B* **2000**, *18*, 301−313.
(15) Huang, R.; Carney, R. P.; Stellacci, F.; Lau, B. L. T. Protein-nanoparticle interactions: the effects of surface compositional and structural heterogeneity are scale dependent. *Nanoscale* **2013**, *5*, 6928−6935.
(16) Nel, A. E.; Mädler, L.; Velegol, D.; Xia, T.; Hoek, E. M. V.; Somasundaran, P.; Klaessig, F.; Castranova, V.; Thompson, M. Understanding biophysicochemical interactions at the nano-bio interface. *Nat. Mater.* **2009**, *8*, 543−557.
(17) Mohammad-Beigi, H.; Hayashi, Y.; Zeuthen, C. M.; Eskandari, H.; Scavenius, C.; Juul-Madsen, K.; Vorup-Jensen, T.; Enghild, J. J.; Sutherland, D. S. Mapping and Identification of Soft Corona Proteins at Nanoparticles and Their Impact on Cellular Association. *Nat. Commun.* **2020**, *11*, 4535.
(18) Moyano, D. F.; Ray, M.; Rotello, V. M. Nanoparticle-Protein Interactions: Water Is the Key. *MRS Bull.* **2014**, *39*, 1069−1073.
(19) Guerrini, L.; Alvarez-Puebla, R.; Pazos-Perez, N. Surface Modifications of Nanoparticles for Stability in Biological Fluids. *Materials* **2018**, *11*, 1154.
(20) Reimhult, E. Nanoparticle Interactions with Blood Proteins and What It Means: A Tutorial Review. *Blood and Genomics* **2019**, *3*, 73−87.
(21) Amstad, E.; Textor, M.; Reimhult, E. Stabilization and Functionalization of Iron Oxide Nanoparticles for Biomedical Applications. *Nanoscale* **2011**, *3*, 2819−2843.
(22) Neoh, K. G.; Kang, E. T. Functionalization of Inorganic Nanoparticles with Polymers for Stealth Biomedical Applications. *Polym. Chem.* **2011**, *2*, 747−759.
(23) Ito, A.; Shinkai, M.; Honda, H.; Kobayashi, T. Medical Application of Functionalized Magnetic Nanoparticles. *J. Biosci. Bioeng.* **2005**, *100*, 1−11.
(24) Tian, Q.; Hu, J.; Zhu, Y.; Zou, R.; Chen, Z.; Yang, S.; Li, R.; Su, Q.; Han, Y.; Liu, X. Sub-10 nm Fe3O4@Cu2-xS Core-Shell Nanoparticles for Dual-Modal Imaging and Photothermal Therapy. *J. Am. Chem. Soc.* **2013**, *135*, 8571−8577.
(25) Premaratne, G.; Dharmaratne, A. C.; Al Mubarak, Z. H.; Mohammadparast, F.; Andiappan, M.; Krishnan, S. Multiplexed Surface Plasmon Imaging of Serum Biomolecules: Fe3O4@Au Core/Shell Nanoparticles with Plasmonic Simulation Insights. *Sens. Actuators, B* **2019**, *299*, 126956.
(26) Gal, N.; Lassenberger, A.; Herrero-Nogareda, L.; Scheberl, A.; Charwat, V.; Kasper, C.; Reimhult, E. Interaction of Size-Tailored PEGylated Iron Oxide Nanoparticles with Lipid Membranes and Cells. *ACS Biomater. Sci. Eng.* **2017**, *3*, 249−259.
(27) Lassenberger, A.; Scheberl, A.; Stadlbauer, A.; Stiglbauer, A.; Helbich, T.; Reimhult, E. Individually Stabilized, Superparamagnetic Nanoparticles with Controlled Shell and Size Leading to Exceptional Stealth Properties and High Relaxivities. *ACS Appl. Mater. Interfaces* **2017**, *9*, 3343−3353.
(28) Kurzhals, S.; Gal, N.; Zirbs, R.; Reimhult, E. Controlled Aggregation and Cell Uptake of Thermoresponsive Polyoxazoline-Grafted Superparamagnetic Iron Oxide Nanoparticles. *Nanoscale* **2017**, *9*, 2793−2805.
(29) Laurent, S.; Forge, D.; Port, M.; Roch, A.; Robic, C.; Vander Elst, L.; Muller, R. N. Magnetic Iron Oxide Nanoparticles: Synthesis, Stabilization, Vectorization, Physicochemical Characterizations, and Biological Applications. *Chem. Rev.* **2008**, *108*, 2064−2110.
(30) Wallyn, J.; Anton, N.; Vandamme, T. F. Synthesis, Principles, and Properties of Magnetite Nanoparticles for In Vivo Imaging Applications-A Review. *Pharmaceutics* **2019**, *11*, 601.
(31) Lewinski, N.; Colvin, V.; Drezek, R. Cytotoxicity of Nanoparticles. *Small* **2008**, *4*, 26−49.
(32) Walkey, C. D.; Chan, W. C. W. Understanding and Controlling the Interaction of Nanomaterials with Proteins in a Physiological Environment. *Chem. Soc. Rev.* **2012**, *41*, 2780−2799.
(33) Mahmoudi, M.; Lynch, I.; Ejtehadi, M. R.; Monopoli, M. P.; Bombelli, F. B.; Laurent, S. Protein−Nanoparticle Interactions: Opportunities and Challenges. *Chem. Rev.* **2011**, *111*, 5610−5637.
(34) Whitwell, H.; Mackay, R.-M.; Elgy, C.; Morgan, C.; Griffiths, M.; Clark, H.; Skipp, P.; Madsen, J. Nanoparticles in the Lung and Their Protein Corona: The Few Proteins That Count. *Nanotoxicology* **2016**, *10*, 1385−1394.
(35) Bouchemal, K. New Challenges for Pharmaceutical Formulations and Drug Delivery Systems Characterization Using Isothermal Titration Calorimetry. *Drug Discovery Today* **2008**, *13*, 960−972.
(36) Bouchemal, K.; Mazzaferro, S. How to conduct and interpret ITC experiments accurately for cyclodextrin-guest interactions. *Drug Discovery Today* **2012**, *17*, 623−629.
(37) Chiad, K.; Stelzig, S. H.; Gropeanu, R.; Weil, T.; Klapper, M.; Müllen, K. Isothermal Titration Calorimetry: A Powerful Technique To Quantify Interactions in Polymer Hybrid Systems. *Macromolecules* **2009**, *42*, 7545−7552.
(38) Freire, E.; Mayorga, O. L.; Straume, M. Isothermal Titration Calorimetry. *Anal. Chem.* **1990**, *62*, 950A−959A.
(39) Tellinghuisen, J. Optimizing Experimental Parameters in Isothermal Titration Calorimetry: Variable Volume Procedures. *J. Phys. Chem. B* **2007**, *111*, 11531−11537.
(40) Tellinghuisen, J. Isothermal Titration Calorimetry at Very Low c. *Anal. Biochem.* **2008**, *373*, 395−397.
(41) Cedervall, T.; Lynch, I.; Lindman, S.; BerggÅrd, T.; Thulin, E.; Nilsson, H.; Dawson, K. A.; Linse, S. Understanding the nanoparticle-protein corona using methods to quantify exchange rates and affinities of proteins for nanoparticles. *PNAS* **2007**, *104*, 2050−2055.
(42) Moyano, D. F.; Saha, K.; Prakash, G.; Yan, B.; Kong, H.; Yazdani, M.; Rotello, V. M. Fabrication of Corona-Free Nanoparticles with Tunable Hydrophobicity. *ACS Nano* **2014**, *8*, 6748−6755.
(43) Gal, N.; Schroffenegger, M.; Reimhult, E. Stealth Nanoparticles Grafted with Dense Polymer Brushes Display Adsorption of Serum Protein Investigated by Isothermal Titration Calorimetry. *J. Phys. Chem. B* **2018**, *122*, 5820−5834.

https://dx.doi.org/10.1021/acsabm.0c01355
ACS Appl. Bio Mater. 2021, 4, 795−806

(44) Schroffenegger, M.; Leitner, N. S.; Morgese, G.; Ramakrishna, S. N.; Willinger, M.; Benetti, E. M.; Reimhult, E. Polymer Topology Determines the Formation of Protein Corona on Core-Shell Nanoparticles. *ACS Nano* **2020**, *14*, 12708−12718.
(45) Morgese, G.; Shirmardi Shaghasemi, B.; Causin, V.; Zenobi-Wong, M.; Ramakrishna, S. N.; Reimhult, E.; Benetti, E. M. Next-Generation Polymer Shells for Inorganic Nanoparticles Are Highly Compact, Ultra-Dense, and Long-Lasting Cyclic Brushes. *Angew. Chem., Int. Ed.* **2017**, *56*, 4507−4511.
(46) Li, S.-D.; Huang, L. Stealth Nanoparticles: High Density but Sheddable PEG Is a Key for Tumor Targeting. *J. Controlled Release* **2010**, *145*, 178−181.
(47) Hoang Thi, T. T.; Pilkington, E. H.; Nguyen, D. H.; Lee, J. S.; Park, K. D.; Truong, N. P. The Importance of Poly(Ethylene Glycol) Alternatives for Overcoming PEG Immunogenicity in Drug Delivery and Bioconjugation. *Polymers* **2020**, *12*, 298.
(48) Wilson, P.; Ke, P. C.; Davis, T. P.; Kempe, K. Poly(2-Oxazoline)-Based Micro- and Nanoparticles: A Review. *Eur. Polym. J.* **2017**, *88*, 486−515.
(49) Sponchioni, M.; Capasso Palmiero, U.; Moscatelli, D. Thermo-Responsive Polymers: Applications of Smart Materials in Drug Delivery and Tissue Engineering. *Mater. Sci. Eng., C* **2019**, *102*, 589−605.
(50) Park, J. H.; Oh, N. Endocytosis and Exocytosis of Nanoparticles in Mammalian Cells. *Int. J. Nanomed.* **2014**, *9*, 51−63.
(51) Raynal, I.; Prigent, P.; Peyramaure, S.; Najid, A.; Rebuzzi, C.; Corot, C. Macrophage Endocytosis of Superparamagnetic Iron Oxide Nanoparticles. *Invest. Radiol.* **2004**, *39*, 56−63.
(52) Gal, N.; Charwat, V.; Städler, B.; Reimhult, E. Poly(Ethylene Glycol) Grafting of Nanoparticles Prevents Uptake by Cells and Transport Through Cell Barrier Layers Regardless of Shear Flow and Particle Size. *ACS Biomater. Sci. Eng.* **2019**, *5*, 4355−4365.
(53) Miglio, A.; Moscati, L.; Scoccia, E.; Maresca, C.; Antognoni, M. T.; Felici, A. Reference Values for Serum Amyloid A, Haptoglobin, Lysozyme, Zinc and Iron in Healthy Lactating Lacaune Sheep. *Acta Vet. Scand.* **2018**, *60*, 46.
(54) Ekdahl, K. N.; Fromell, K.; Mohlin, C.; Teramura, Y.; Nilsson, B. A Human Whole-Blood Model to Study the Activation of Innate Immunity System Triggered by Nanoparticles as a Demonstrator for Toxicity. *Sci. Technol. Adv. Mater.* **2019**, *20*, 688−698.
(55) Schöttler, S.; Becker, G.; Winzen, S.; Steinbach, T.; Mohr, K.; Landfester, K.; Mailänder, V.; Wurm, F. R. Protein Adsorption Is Required for Stealth Effect of Poly(Ethylene Glycol)- and Poly-(Phosphoester)-Coated Nanocarriers. *Nat. Nanotechnol.* **2016**, *11*, 372−377.
(56) Gasteiger, E.; Hoogland, C.; Gattiker, A.; Duvaud, S.; Wilkins, M. R.; Appel, R. D.; Bairoch, A. Protein Identification and Analysis Tools on the ExPASy Server. In *The Proteomics Protocols Handbook*; Walker, J. M., Ed.; Springer Protocols Handbooks; Humana Press: Totowa, NJ, 2005; pp 571−607.
(57) Amstad, E.; Gillich, T.; Bilecka, I.; Textor, M.; Reimhult, E. Ultrastable Iron Oxide Nanoparticle Colloidal Suspensions Using Dispersants with Catechol-Derived Anchor Groups. *Nano Lett.* **2009**, *9*, 4042−4048.
(58) Mohammed, L.; Gomaa, H. G.; Ragab, D.; Zhu, J. Magnetic Nanoparticles for Environmental and Biomedical Applications: A Review. *Particuology* **2017**, *30*, 1−14.
(59) Marsh, D.; Bartucci, R.; Sportelli, L. Lipid Membranes with Grafted Polymers: Physicochemical Aspects. *Biochim. Biophys. Acta, Biomembr.* **2003**, *1615*, 33−59.
(60) Su, H.; Xu, Y. Application of ITC-Based Characterization of Thermodynamic and Kinetic Association of Ligands With Proteins in Drug Design. *Front. Pharmacol.* **2018**, *9*. DOI: 10.3389/fphar.2018.01133.
(61) Zirbs, R.; Lassenberger, A.; Vonderhaid, I.; Kurzhals, S.; Reimhult, E. Melt-grafting for the synthesis of core-shell nanoparticles with ultra-high dispersant density. *Nanoscale* **2015**, *7*, 11216−11225.
(62) Quinlan, G. J.; Martin, G. S.; Evans, T. W. Albumin: Biochemical Properties and Therapeutic Potential. *Hepatology* **2005**, *41*, 1211−1219.
(63) Marichal, L.; Degrouard, J.; Gatin, A.; Raffray, N.; Aude, J.-C.; Boulard, Y.; Combet, S.; Cousin, F.; Hourdez, S.; Mary, J.; Renault, J.-P.; Pin, S. From Protein Corona to Colloidal Self-Assembly: The Importance of Protein Size in Protein-Nanoparticle Interactions. *Langmuir* **2020**, *36*, 8218−8230.
(64) Prozeller, D.; Morsbach, S.; Landfester, K. Isothermal Titration Calorimetry as a Complementary Method for Investigating Nanoparticle-Protein Interactions. *Nanoscale* **2019**, *11*, 19265−19273.
(65) Bixner, O.; Lassenberger, A.; Baurecht, D.; Reimhult, E. Complete Exchange of the Hydrophobic Dispersant Shell on Monodisperse Superparamagnetic Iron Oxide Nanoparticles. *Langmuir* **2015**, *31*, 9198−9204.
(66) Davis, K.; Cole, B.; Ghelardini, M.; Powell, B. A.; Mefford, O. T. Quantitative Measurement of Ligand Exchange with Small-Molecule Ligands on Iron Oxide Nanoparticles via Radioanalytical Techniques. *Langmuir* **2016**, *32*, 13716−13727.
(67) Eisenberg, D.; Schwarz, E.; Komaromy, M.; Wall, R. Analysis of Membrane and Surface Protein Sequences with the Hydrophobic Moment Plot. *J. Mol. Biol.* **1984**, *179*, 125−142.
(68) Baker, N. A.; Sept, D.; Joseph, S.; Holst, M. J.; McCammon, J. A. Electrostatics of Nanosystems: Application to Microtubules and the Ribosome. *Proc. Natl. Acad. Sci. U.S.A.* **2001**, *98*, 10037−10041.
(69) Baker, H. M.; Baker, E. N. A structural perspective on lactoferrin function1This article is part of a Special Issue entitled Lactoferrin and has undergone the Journal's usual peer review process. *Biochem. Cell Biol.* **2012**, *90*, 320−328.
(70) McPeak, K. M.; van Engers, C. D.; Bianchi, S.; Rossinelli, A.; Poulikakos, L. V.; Bernard, L.; Herrmann, S.; Kim, D. K.; Burger, S.; Blome, M.; Jayanti, S. V.; Norris, D. J. Ultraviolet Plasmonic Chirality from Colloidal Aluminum Nanoparticles Exhibiting Charge-Selective Protein Detection. *Adv. Mater.* **2015**, *27*, 6244−6250.

https://dx.doi.org/10.1021/acsabm.0c01355
ACS Appl. Bio Mater. 2021, 4, 795−806